Liquid-Crystal-Tuned Resonant Series Patch Array With Unique Element Spacing Emulating Simplified Operating Construe of Traveling-Wave Antenna

Jaehoon Kim, *Student Member, IEEE*, Woojun Lee, *Student Member, IEEE*, and Jungsuek Oh, *Senior Member, IEEE*

***Abstract*—This letter presents a liquid crystal (LC) tuned resonant series patch array that interpretively emulates simplified unidirectional traveling-wave operation by eliminating the dependency on the undesirably tuned reflection coefficient. The general term for the resonantly excited current of a series-fed topology involving the reflection coefficient is derived. Additionally, a newly defined array factor is introduced, incorporating LC-tuned reconfigurability of constituent unit elements. Furthermore, a unique element spacing that has been rebuffed in broadside arrays due to out-of-phase radiation is selected for improved scanning performance despite a confined phase-tuning range and simplified noniterative analysis. Moreover, the impedance matching procedure that successfully maintains the input matched condition against variations in the LC dielectric constant is established by modifying the slotted coupling topology. It is demonstrated that a significantly enhanced gain of 12.1 dBi and aperture efficiency of 30.1% are achieved at 28.5 GHz compared to previously studied counterparts for which measured results are unavailable, and huge loss is inevitably accompanied by topological limitations.**

***Index Terms*—Array factor, impedance matching, liquid crystal, reflection coefficient, resonant, series patch array.**

I. Introduction

RECENTLY the commercialization of millimeter-wave (mmWave) 5G has emerged [1], [2], [3], [4]. However, most manufacturers have technical difficulties in feasible supply due to practical issues, such as the small-sized integration of beamforming antenna modules and corresponding heat generation caused by rapidly increasing RF loss at high-frequencies. Accordingly, vibrant research on reconfigurable beamforming antennas (RBAs) that can substitute radio frequency integrated circuit (RFIC) based beamforming antennas, which can be limited in use at upcoming higher frequencies is being conducted. Among reconfigurable components, liquid crystals (LCs) gain an advantage of operability and comparably reasonable loss at high-frequencies over other candidates. Despite its relatively slow response time ranging from msec to sec, LC can be utilized in various 5G use cases such as fixed wireless access, where fast switching is not required. However, the successful maintenance of radiating performance and detailed operating analysis of LC-tuned RBAs with constantly changing LC dielectric constants has been limited so far. Despite this tough condition, several studies have attempted to design LC-based resonant RBAs [5], [6], [7], [8], [9], [10], [11]. In [5], an LC-based power divider (PD) is utilized for the isolated design of radiating elements to be analyzed independently, which is not preferred in terms of aperture efficiency (AE) due to the extended RF path. In [6], [7], [8], and [9], meander lines (MLs) and reflective phase shifters (RPSs) with PDs are employed to maximize the constrained phase-tuning range (PTR) of the LC, but low AE could not be overcome. In [10], a series-fed topology without PDs is employed, along with interelement RPSs. However, the operating principle for unisolated series-fed elements was not analyzed, and low AE is not overcome.

Therefore, this letter proposes an LC-based resonant series patch array (RSPA) without lossy PDs combined with MLs and RPSs for enhanced performance employing a simplified methodology by removing the interpretative dependency on the reflection coefficient (Γ) like unidirectional traveling-wave. In Section II, the design methodology of the LC-tuned RSPA is presented. In Section III, the simulated and measured results of a 1×10 RSPA employing the approach described in Section II is presented. Finally, Section IV concludes this letter.

II. Design Methodology of LC-Based RSPA

A. Derivation of Array Factor Based on Traveling-Wave-Like Resonant Operation

Fig. 1(a) shows the single unit antenna for analyzing unit elements (UEs) in RSPA. The feeding part of the antenna is a straight microstrip line. The H-shaped slot is located on the ground (GND) to couple the feed wave with the upper patches. The LC with a variable dielectric constant ($\varepsilon_{\mathrm{LC}}$) is sandwiched between the GND and the bottom patch, and it is enclosed inside Substrate 2, which has a perforated cavity. In this letter, the GT7-29001 from Merck, which has a dielectric constant range of 2.5–3.5 and a corresponding loss tangent of 0.0116–0.0064 is employed. The line connected to the bottom patch is in contact with the dc pad through a metal via. Dc voltage will be applied to the pad to tune the LC in measurements. The top patch is stacked on Substrate 1 for gain enhancement under the same height conditions, but not for dual-band operation. The dielectric used in the three substrates is TLY-5 from Taconic, which has a dielectric constant of 2.2 and a loss tangent of

Manuscript received 24 July 2023; revised 21 August 2023; accepted 28 August 2023. Date of publication 31 August 2023; date of current version 1 December 2023. This work was supported by SAMSUNG Research, Samsung Electronics Company, Ltd. *(Corresponding author: Jungsuek Oh.)*

The authors are with the School of Electrical and Computer Engineering, Institute of New Media Communication, Seoul National University, Seoul 152-742, South Korea (e-mail: jaehoonkim@snu.ac.kr; xxzwwe30@gmail.com; jungsuek@snu.ac.kr).

Digital Object Identifier 10.1109/LAWP.2023.3310496

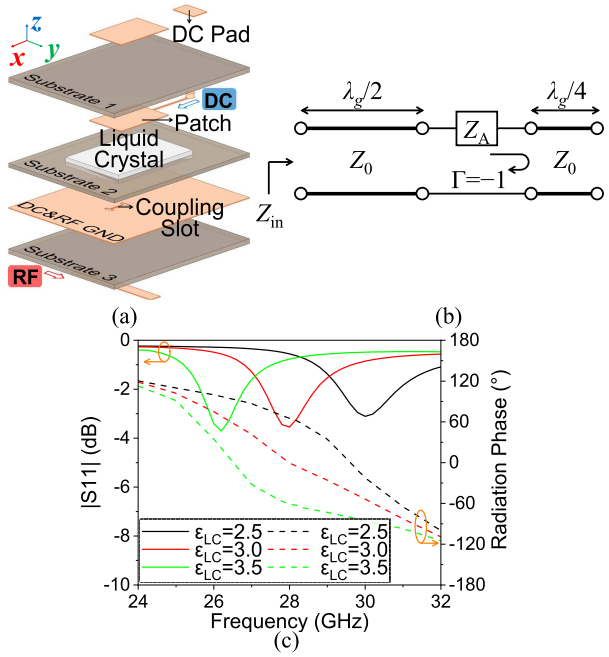

Fig. 1. (a) Single unit antenna for analyzing UEs constituting RSPA, (b) its EC, and (c) its $|S_{11}|$ and radiating phase for ε_{LC}.

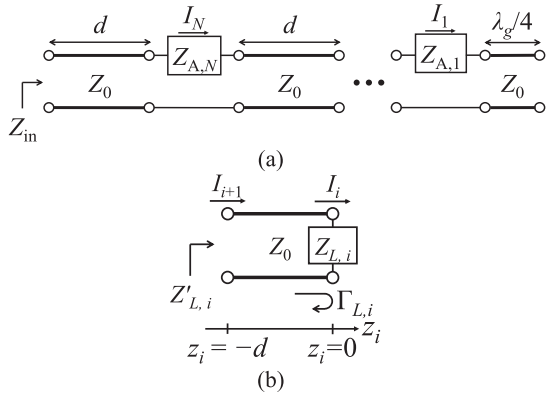

Fig. 2. (a) EC of a one-dimensional aperture-coupled RSPA with $\lambda_g/4$ open-ended termination and (b) modified EC for calculating reflection coefficient of each antenna stage.

0.0009. The thickness of Substrate 2 is 0.13 mm whereas that of Substrates 1 and 3 is 0.25 mm. Three PCB layers are bonded using Tacbond 1.5 from Taconic, with a thickness of 0.04 mm. Fig. 1(b) shows the equivalent circuit (EC) of Fig. 1(a), where Z_A is the antenna impedance, Z_0 is the characteristic impedance of the transmission line (TRL), Z_{in} is the input impedance, Γ is the reflection coefficient of the antenna stage, and λ_g is the guided wavelength. Z_A is calculated using Z_{in} since these two values are identical by the TRL theory [12]. Fig. 1(c) shows the $|S_{11}|$ and radiating phase of the UE for ε_{LC}. Note that the resonant frequency decreases as ε_{LC} increases, resulting in the tuning of the radiating phase near 28 GHz.

Fig. 2(a) shows the EC of the 1-D aperture-coupled RSPA with $\lambda_g/4$ open-ended termination, where d is the element spacing, $Z_{A,i}$ is the antenna impedance of ith UE, and I_i is the excited current of ith UE. A series-fed straight TRL without a PD and RPS is considered in the proposed RSPA. N UEs constituting the RSPA are connected in series with each TRL [13]. Fig. 2(b) shows the modified EC of Fig. 2(a) for calculating I_i, where $Z_{L,i}$ is the equivalent load impedance of the ith UE stage, $Z'_{L,i}$ is the input impedance of the TRL with $Z_{L,i}$ load, and $\Gamma_{L,i}$ is the reflection coefficient of the ith UE stage. $\Gamma_{L,i}$ is expressed as (1)–(3), where β is the propagation constant of the TRL [13]

$$\Gamma_{L,i} = \frac{Z_{L,i} - Z_0}{Z_{L,i} + Z_0} \tag{1}$$

$$Z_{L,i} = Z_{A,i} + Z'_{L,i-1} \tag{2}$$

$$Z'_{L,i-1} = Z_0 \frac{Z_{L,i-1} + jZ_0 \tan \beta d}{Z_0 + jZ_{L,i-1} \tan \beta d}. \tag{3}$$

By taking the ratio of I_{i+1}/I_i using the $\Gamma_{L,i}$ in (1) by the TRL theory, an iterative expression for the current at successive points along the array is derived as

$$I_{i+1} = I_i \cdot \frac{1 - \Gamma_{L,i} e^{-j2\beta d}}{1 - \Gamma_{L,i}} e^{j\beta d}. \tag{4}$$

When the lossless case is assumed, $|I_1|$ can be normalized to 1 because it is located at the peak amplitude of the standing wave of the TRL due to the $\lambda_g/4$ open-ended topology. Thus, when the reference phase of I_1 is assumed to be 0° ($I_1 = e^{j0}$), the general term of I_i ($2 \le i \le N$) can be expressed as

$$I_i = \prod_{i'=1}^{i-1} \left[\frac{1 - \Gamma_{L,i'} e^{-j2\beta d}}{1 - \Gamma_{L,i'}} e^{j\beta d} \right]. \tag{5}$$

Therefore, iterative calculation is inevitably required to analyze the magnitude and phase of I_i at each UE stage of the LC-tuned RSPA. Moreover, $\Gamma_{L,i}$ undesirably changes based on the variable ε_{LC} of each UE to achieve arbitrarily desired main lobe directions. Thus, to address this complexity, the element spacing, $d = \lambda_g/2 \times n$, where n is a positive integer that satisfies the condition of $e^{-j2\beta d} = 1$, is proposed for simplified construe. With this approach, the I_i in the RSPA is significantly simplified to (6), emulating that of unidirectional traveling-wave regardless of the variable $\Gamma_{L,i}$, where x_i denotes $(i-1)d$

$$I_i = e^{j\beta x_i}. \tag{6}$$

Note that the intriguing spacing of $d = \lambda_g/2$, at which the I_i of every adjacent UE satisfy the out-of-phase radiation, is chosen for enhanced scanning performance, in contrast to most previous works where all I_i have an equal phase for in-phase broadside radiation at the reference LC state where all UEs have the same value of ε_{LC}. In that condition, more advanced scanning performance can be achieved in the LC-tuned RSPA with narrow PTR of 140°, as shown in Fig. 1(c).

Thus, the array factor (AF) of the RSPA is expressed as (7), where k is the wavenumber in free space, A_i is the normalized current excitation coefficient of each UE, and α_i is the normalized reconfigurability of the LC-tuned UE

$$\text{AF} = \sum_{i=1}^{N} A_i e^{jkx_i \sin\theta} = \sum_{i=1}^{N} I_i \alpha_i e^{jkx_i \sin\theta}$$

$$= \sum_{i=1}^{N} \alpha_i e^{j\beta x_i} e^{jkx_i \sin\theta}. \tag{7}$$

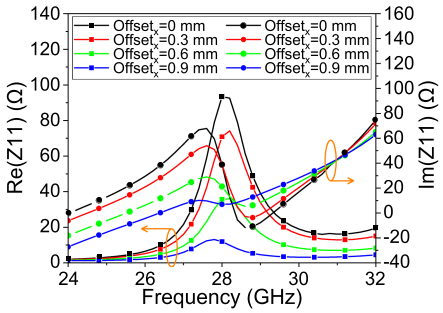

Fig. 3. Input impedance of Fig. 1(b) according to Offset$_x$.

The first maxima of (7) in the desired direction θ_0 occurs when (8) is satisfied [14]

$$\angle\alpha_i = -\beta x_i - kx_i \sin\theta_0. \tag{8}$$

However, the proposed UE has a limited PTR of 140°. Therefore, a phase compensating method, which downscales the ideally required value of (8) to a constrained value of (9) with the approximated α_i ($\alpha_{i,\text{approx}}$) is proposed where R_{unit} is the PTR of the employed UE

$$\angle\alpha_{i,\text{approx}} = \angle\alpha_i \times \frac{R_{\text{unit}}}{360^\circ}. \tag{9}$$

Interestingly, when $d = \lambda_g/2$ is paired with (9), it can collimate the main lobe in any θ_0, as described in the following section.

The radiating power of each UE is expressed as

$$P_{\text{rad},i} = |I_i|^2 \cdot \text{Re}\left(Z_{\text{A},i}\right)/2. \tag{10}$$

Since all $|I_i|$ are equal by (6), $|A_i|$ is expressed as

$$|A_i| = |\alpha_{i,\text{approx}}| \propto \sqrt{\text{Re}\left(Z_{A,i}\right)}. \tag{11}$$

Therefore, the AF, which considers both the magnitude and the phase of A_i is numerically calculated in the following section based on the impedance analysis of the final configuration of the UE in a 1 × 10 RSPA.

B. Impedance Matching and Numerically Calculated AF

Herein, the EC of Fig. 2(a) is utilized for impedance matching of the proposed 1 × 10 RSPA. Under the $d = \lambda_g/2$ condition, the TRL with a length d becomes transparent, and the $\lambda_g/4$ open-ended output stage is equivalent to a short circuit [12]. Thus, all UEs are connected in series, and the input impedance can be expressed as

$$Z_{\text{in}} = \sum_{i=1}^{N} Z_{\text{A},i}. \tag{12}$$

Therefore, successful matching can be achieved by employing a UE with a smaller antenna impedance than that of a single unit antenna. Fig. 3 shows the Z_{A} of Fig. 1(b) for the median value of the ε_{LC} range (3.0) according to Offset$_x$, which is defined in the same manner as that shown in Fig. 5. Note that the real and imaginary parts of the antenna impedance decrease as Offset$_x$ increases. Thus, Offset$_x$ of 0.9 mm is selected to ensure the consistent maintenance of the input matched condition at the targeted 28 GHz despite the variation in each LC dielectric constant ($\varepsilon_{\text{LC},i}$) in Fig. 5 for any θ_0. Although omitted, the Z_{A} of the UE in that condition is small and has a gradual slope, making it nearly invariant for ε_{LC}. Note that Fig. 1(c) is the result of the single unit antenna with Offset$_x$ = 0.9 mm for the optimized UE of the RSPA, so input matching is poorly achieved.

TABLE I
DISCRETIZED APPROXIMATED RECONFIGURABILITY ($\alpha_{i,\text{approx}}$) OF A UNIT ELEMENT ACCORDING TO IDEALLY REQUIRED PHASE

$\angle\alpha_i$	[−180, −108]	[−108, −36]	[−36, 36]	[36, 108]	[108, 180]
$\angle\alpha_{i,\text{approx}}$	−70°	−35°	−0°	35°	70°
$\lvert\alpha_{i,\text{approx}}\rvert$	0.43	0.78	1	0.89	0.45
$\varepsilon_{\text{LC},i}$	3.5	3.2	3.0	2.8	2.5

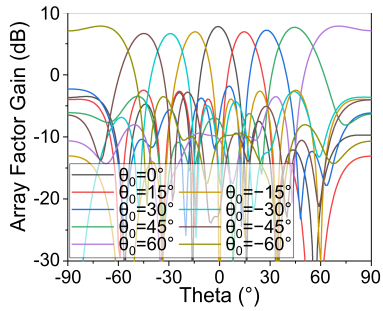

Fig. 4. AF of a 1 × 10 RSPA with $d = \lambda_g/2$ and approximated α_i ($\alpha_{i,\text{approx}}$) of 10 LC-tuned UEs.

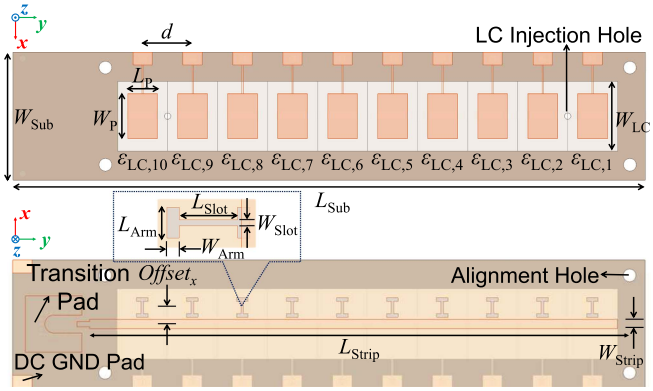

Fig. 5. Drawings of a 1 × 10 RSPA and its design parameters.

Furthermore, the $|\alpha_{i,\text{approx}}|$ can be extracted by the Z_{in} of Fig. 1(b) using (11) with the final topology of the UE. The $\alpha_{i,\text{approx}}$ is discretized into five states, as shown in Table I, considering the practical implementation of the control circuit. $|\alpha_{i,\text{approx}}|$ with $\varepsilon_{\text{LC}} = 3.0$, which has the maximum resistance at the target frequency is normalized to 1. Fig. 4 shows the AF of the 1 × 10 RSPA calculated by (7) with the $d = \lambda_g/2$ condition and $\alpha_{i,\text{approx}}$ of 10 UEs. Note that enhanced scanning performance with relatively uniform gain and minor lobe level is achieved at all θ_0 despite the constrained PTR of the LC-tuned UE.

III. Simulation and Measurement Results

Fig. 5 shows the drawings of a 1 × 10 RSPA and its design parameters. Table II lists these parameters and their values. Three PCBs, constituting each layer of the RSPA, were fabricated individually. Then, the PCBs were stacked with bondplies that had been machined to the same shape as the cavity-perforated Substrate 2. Finally, LC was injected through the injection hole

TABLE II
DESIGN PARAMETERS AND THEIR VALUES OF A 1 × 10 RSPA

Parameters & Values							
W_{Sub}	10	W_{Slot}	0.1	Offset$_x$	0.9	d	3.9
L_{Sub}	49.2	L_{Slot}	0.95	W_{Strip}	0.75	W_{LC}	5.5
W_P	3.5	W_{Arm}	0.2	L_{Strip}	41		
L_P	2.3	L_{Arm}	0.5	W_{LC}	5.5		

(Unit : mm)

TABLE III
COMPARISON BETWEEN PRIOR LC-BASED RESONANT RBAS AND THE PROPOSED 1 × 10 RSPA

Ref	f_0 (GHz)	Feeding Configuration	3 dB Scan Range (°)	Measured Gain (dBi)	Measured AE (%)
[5]	28	PD	0 –30	N/A	N/A
[6]	14.5	PD+ML	−20 – 20	N/A	N/A
[7]	28.4	PD+ML	−40 – 40	4.5	3
[8]	10	PD+ML	−25 – 25	N/A	N/A
[9]	35	Multi-Channel+RPS	−22 – 23	6.7	1.6
[10]	63.5	Single-Channel+RPS	8 – 35	N/A	N/A
[11]	28	Single-Channel	−27 – 29	6	9.6
This Work	28.5	Single-Channel	−30 – 30	12.1	30.1

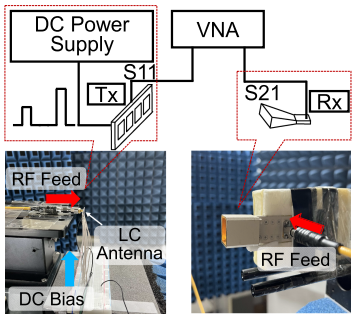

Fig. 6. Antenna measurement setup and its schematic.

drilled in the upper PCB, and both holes were sealed with epoxy. The multilayer topology designed to effectively enclose LC has limitations in achieving a low-profile design; however, it features a substantial dielectric volume, which leads to a reduction in the effective resonant length of the radiating patches (L_P). Therefore, there is an advantage in reducing unexpected mutual coupling between adjacent UEs. Fig. 6 shows the experimental setup of the proposed antenna and its schematics. A standard horn operating at Ka-band is used as the Rx antenna. A 2-port vector network analyzer is used to measure the $|S_{11}|$ and E-plane radiation patterns. A dc power supply is used to apply individual dc voltages to each pad. A single unit antenna with the same values of the physical parameters as those of the UEs in the 1 × 10 RSPA is fabricated to extract the ε_{LC} by applying dc voltage and using the curve fitting method between simulated and measured $|S_{11}|$ [16]. The dc voltage values for ε_{LC} of 2.5, 2.8, 3.0, 3.2, and 3.5 are 0, 4.1, 5.4, 9.5, and 20 V, respectively. Fig. 7 shows the simulated and measured $|S_{11}|$ of a 1 × 10 RSPA

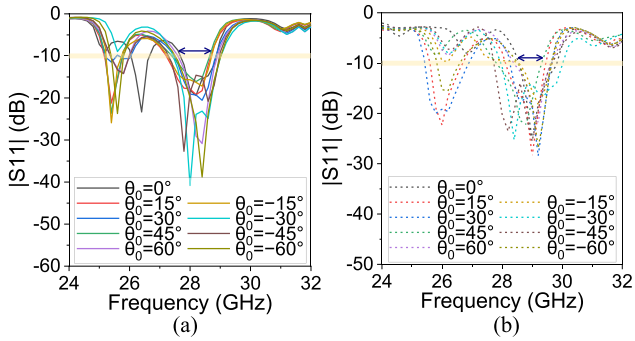

Fig. 7. (a) Simulated and (b) measured $|S_{11}|$ of a 1 × 10 RSPA.

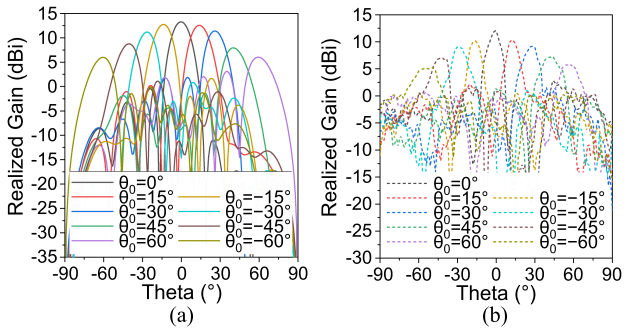

Fig. 8. (a) Simulated and (b) measured 2-D radiation patterns of a 1 × 10 RSPA on the E-plane.

for θ_0. Simulated and measured −10 dB commonly matched impedance bandwidths of 27.7–28.8 and 28.3–29.3 GHz are achieved as indicated by the horizontal arrows despite the variation of $\varepsilon_{LC,i}$. Fig. 8 shows the simulated and measured radiation patterns. Simulated and measured broadside gains of 13.2 and 12.1 dBi are achieved. Slight errors in terms of frequency deviation and gain degradation are estimated due to errors in $\varepsilon_{LC,i}$ by the dc voltage owing to field interference between adjacent elements and an immature bonding process with the drilled PCB, which has not been commercialized. Table III presents a comparison between the proposed LC-based resonant RBA and prior approaches. While most previous works utilized multichannel or PDs combined with lossy MLs and RPSs to overcome the constrained PTR of the LC, the proposed RSPA utilizes a single-channel straight line. Therefore, the proposed RSPA achieves significantly enhanced AE compared to existing designs that reported insufficient gain or failed to attain measured results due to unfeasible topologies with fluidic LC.

IV. CONCLUSION

This letter presents an AE-enhanced RSPA employing a simplified equation of a traveling-wave like form. The proposed methodology establishes a new general term for the resonantly excited current. Moreover, the element spacing that has been avoided due to out-of-phase radiation in broadside array is selected for enhanced scanning despite the narrow PTR as well as simplified operating analysis. This letter can be an invaluable asset for next-generation RBAs at upcoming higher frequencies, where the manufacturing, integration, and production of RFICs are technically limited.

REFERENCES

[1] A. Gaebler et al., "Liquid crystal-reconfigurable antenna concepts for space applications at microwave and millimeter waves," *Int. J. Antennas Propag.*, vol. 2009, Feb. 2009, Art. no. 876989, doi: 10.1155/2009/876989.

[2] S. L. Gunamony, J. B. Gnanadhas, and D. E. Lawrence, "Design and investigation of a miniaturized single-layer ACS-fed dual band antenna for LTE and 5G applications," *J. Electromagn. Eng. Sci.*, vol. 20, no. 3, pp. 213–220, Jul. 2020.

[3] W. A. Awan, S. I. Naqvi, A. H. Naqvi, S. M. Abbas, A. Zaidi, and N. Hussain, "Design and characterization of wideband printed antenna based on DGS for 28 GHz 5G applications," *J. Electromagn. Eng. Sci.*, vol. 21, no. 3, pp. 177–183, Jul. 2021.

[4] R. Shanmugam, "Design and analysis of a frequency reconfigurable penta-band antenna for WLAN and 5G applications," *J. Electromagn. Eng. Sci.*, vol. 21, no. 3, pp. 228–235, Jul. 2021.

[5] M. Nestoros, N. C. Papanicolaou, and A. C. Polycarpou, "Design of beam-steerable array for 5G applications using tunable liquid-crystal phase shifters," in *Proc. 13rd Eur. Conf. Antennas Propag.*, 2019, pp. 1–4.

[6] Y. Zhao, C. Huang, A.-Y. Qing, and X. Luo, "A frequency and pattern reconfigurable antenna array based on liquid crystal technology," *IEEE Photon. J.*, vol. 9, no. 3, Jun. 2017, Art. no. 4600307.

[7] D. Wang, E. Polat, H. Tesmer, R. Jakoby, and H. Maune, "A compact and fast 1×4 continuously steerable endfire phased-array antenna based on liquid crystal," *IEEE Antennas Wireless Propag. Lett.*, vol. 20, no. 10, pp. 1859–1862, Oct. 2021.

[8] A. Mehmood et al., "Dielectric resonator antenna phased array with liquid crystal based phase shifters," in *Proc. 8th Eur. Conf. Antennas Propag.*, 2014, pp. 2436–2439.

[9] X. Y. Li, D. Jiang, J. Liu, and M. S. Tong, "A Ka-band multilayer beaming-scanning antenna using liquid crystals," *IEEE Antennas Wireless Propag. Lett.*, vol. 21, no. 1, pp. 44–48, Jan. 2022.

[10] P. Deo, D. Mirshekar-Syahkal, L. Seddon, S. E. Day, and F. A. Fernández, "60 GHz liquid crystal phased array using reflection-type phase shifter," in *Proc. Eur. Conf. Antennas Propag.*, 2013, pp. 927–929.

[11] J. Shu, G. Xu, H. Peng, and J. Mao, "An electrically steerable parasitic array radiator in package based on liquid crystal," *IEEE Antennas Wireless Propag. Lett.*, vol. 18, no. 11, pp. 2365–2369, Nov. 2019.

[12] D. M. Pozar, *Microwave Engineering*, 3rd ed. Hoboken, NJ, USA: Wiley, 2005.

[13] A. N. Tulintseff, "Series-fed-type linear arrays of dipole and slot elements transversely coupled to a microstrip line," in *Proc. IEEE Antennas Propag. Soc. Int. Symp.*, 1993, vol. 1, pp. 128–131, doi: 10.1109/APS.1993.385386.

[14] C. A. Balanis, *Antenna Theory: Analysis and Design*. Hoboken, NJ, USA: Wiley, 2005.

[15] D. R. Smith, O. Yurduseven, L. P. Mancera, P. Bowen, and N. B. Kundtz, "Analysis of a waveguide-fed metasurface antenna," *Phys. Rev. Appl.*, vol. 8, no. 5, Nov. 2017, Art. no. 054048.

[16] J. Kim and J. Oh, "Liquid-crystal-embedded aperture-coupled microstrip antenna for 5G applications," *IEEE Antennas Wireless Propag. Lett.*, vol. 19, no. 11, pp. 1958–1962, Nov. 2020, doi: 10.1109/LAWP.2020.3014715.